Journal of Colloid and Interface Science 386 (2012) 240–251

Contents lists available at SciVerse ScienceDirect

Journal of Colloid and Interface Science

www.elsevier.com/locate/jcis

Conductivity in nonpolar media: Experimental and numerical studies on sodium AOT–hexadecane, lecithin–hexadecane and aluminum(III)-3,5-diisopropyl salicylate–hexadecane systems

Jochen Schmidt [a], Rodolphe Prignitz [b], Dirk Peschka [c], Andreas Münch [d], Barbara Wagner [e], Eberhard Bänsch [b,*], Wolfgang Peukert [a,*]

[a] Institute of Particle Technology, University of Erlangen-Nuremberg, Cauerstr. 4, 91058 Erlangen, Germany
[b] Department Mathematics, Applied Mathematics 3, University of Erlangen-Nuremberg, Cauerstr. 11, 91058 Erlangen, Germany
[c] Weierstrass Institute for Applied Analysis and Stochastics, Mohrenstr. 39, 10117 Berlin, Germany
[d] Mathematical Institute, University of Oxford, 24–29 St. Giles', Oxford OX1 3LB, UK
[e] Department of Mathematics, Technische Universität Berlin, Straße des 17. Juni 136, 10623 Berlin, Germany

ARTICLE INFO

Article history:
Received 19 April 2012
Accepted 18 July 2012
Available online 1 August 2012

Keywords:
Direct numerical simulation
Finite element analysis
Poisson–Nernst–Planck model
Electrochemical impedance spectroscopy
Degree of dissociation
Reverse micelles

ABSTRACT

The conductivity behavior of doped hydrocarbon systems is studied by applying impedance spectroscopy. In the case of 3,5-diisopropyl salicylato aluminum (III) the charge carriers are formed by dissociation of the compound and their concentration is proportional to the square root of the solute concentration. In hydrocarbon systems that consist of micelle forming compounds (sodium AOT/ lecithin) a linear dependence of charge carrier concentration on solute concentration is observed in the concentration regime where micelles are present.

The conduction mechanisms are studied by numerical solution of a Poisson–Nernst–Planck system that describes the charge transport. We follow two different approaches to extract the degree of micelle dissociation from the impedance data. Firstly, by computing the response of a linear approximation of the Poisson–Nernst–Planck model, and secondly by computing the fully nonlinear response from direct numerical simulations using finite elements. For high and moderate frequencies both approaches agree very well with the experimental data. For small frequencies the response becomes nonlinear and the concept of impedance fails. Furthermore, the numerically computed values for the degree of dissociation are of the same order of magnitude as the values obtained with classical formulas, but still differ by a factor of about 1/3. The direct numerical simulation allows new insight into the conduction mechanisms for different frequency regimes.

1. Introduction

Several practical applications have been recognized for years where tailoring electrical conductivity of hydrocarbon systems is essential. A detailed understanding of ionics and charge generation in nonaqueous systems is needed to develop successful strategies for stabilizing nonpolar dispersions by tailoring particle particle interactions [1–5]. Frequently, compounds that may enhance hydrocarbon conductivity will influence particle charging. These so-called charge control agents are used as an additive for the dispersion formulation of ink-jet printing and liquid toner systems [6,7]. They are used to stabilize soot particles in engine oils [8,9] or for application in electrophoretic displays [10]. Moreover, such compounds are indispensable additives in fuels to prevent electrostatic charging during handling.

Although the underlying mechanisms of ionic conduction in aqueous environment are well-known there still is considerable controversy about charge transport and charge generation in nonpolar environment. In pure nonpolar media charge transport due to a hopping mechanism of photo-generated electrons has been reported [11,12]. In the case of doped hydrocarbons charged reverse micelles have been identified to act as charge carriers in nonpolar environment [1,13,4,14]. In this case the generation of charge carriers and charge carrier size will be strongly influenced by the amount of residual water present in the system [15]. For long-chained alkanes experimental conductivity data exist that differ by orders of magnitude. The reasons for these differences in conductivity are obvious: even traces of polar impurities that are dissolved in the hydrocarbon may enhance the conductivity considerably.

Within the experimental section of this article the impedance behavior of a nonpolar solvent doped with charge control agents,

* Corresponding authors. Fax: +49 9131 8529402 (W. Peukert), +49 9131 8567201 (E. Bänsch).
E-mail addresses: baensch@am.uni-erlangen.de (E. Bänsch), w.peukert@lfg.uni-erlangen.de (W. Peukert).

0021-9797/$ - see front matter © 2012 Elsevier Inc. All rights reserved.
http://dx.doi.org/10.1016/j.jcis.2012.07.051

i.e. the micellar system lecithin (α-phosphatidylcholine)-hexadecane and hexadecane solutions of an aluminum salicylic acid complex compound (3,5-diisopropyl salicylato aluminum (III)) is addressed and compared to data obtained for the well characterized micellar hydrocarbon-sodium AOT system [16,17]. The concentration dependent conductivity behavior of the aforementioned systems is described by simple chemical equilibrium considerations.

Further insights into our experimental results including the spatial distribution of ions are achieved by the formulation and solution of an appropriate model describing the system. For small concentrations we set up a time-dependent version of the Poisson–Nernst–Planck (PNP) model coupled to the Stokes equation. For an introduction to the PNP model we refer to [18–22] and references therein.

Simulations are done for the lecithin–hexadecane system. Within the simulations the impedance calculated is fitted to the measured data of the system to determine the degree of dissociation. The simulations were performed for a linearized time-periodic version of the PNP-system and for the full nonlinear model. A short derivation of the numerical method, including a justification of the algorithms used, is given in the numerical section of this article.

Finally, we show that the values of the degree of dissociation of charged micelles are of the same order of magnitude as the values estimated from simple equilibrium considerations. Differences in impedance behavior of micellar systems (AOT, lecithin) and the aluminum salicylate system are also discussed and the cmc regions of AOT and lecithin in hexadecane system are determined.

2. Experimental

2.1. Instrumental and chemicals used

Impedance analyses of solutions of AOT sodium salt (NaAOT) in hexadecane, 3,5-diisopropyl salicylato aluminum (III) (Al (dips)$_3$) in hexadecane and lecithin in hexadecane, respectively, have been carried out using the dielectric spectrometer Alpha-Analyzer (Novocontrol) equipped with a ZGS head. Solutions were prepared by dissolving appropriate amounts of AOT sodium salt, Al (dips)$_3$ or lecithin (Fluka, 99%), respectively, in hexadecane (95%, Alfa Aesar) at room temperature. The water content of the hydrocarbon has been determined to be (67.5 ± 2.8) mg/kg using the coulometric Karl-Fischer titration device 720 KFS Titrino (Metrohm). Unless otherwise stated the chemicals have been used without any further purification. Prior to use the AOT sodium salt (Acros, 96%) has been purified by re-crystallization from methanol (Roth, ⩾99.5% Ph. Eur.). The solutions were allowed to equilibrate for at least 24 h at room temperature prior to impedance measurements. The solutions have been introduced into a cylindrical sample cell (BDS1307, Novocontrol) connected to the impedance analyzer. Measurements have been performed at temperatures between 20 °C and 70 °C in the frequency range 10^{-4} Hz to 20 MHz (at 1 V (root mean square)) in nitrogen atmosphere. Before performing the measurements the sample cell has been thoroughly flushed with the sample solution and has been equilibrated at the destined temperature for 30 min which was sufficient to attain thermal equilibrium. The temperature has been maintained constant during impedance characterization with an accuracy of 0.1 K by purging with dry nitrogen gas flow of desired temperature using the Quatro Cryosystem (Novocontrol). Impedance data have been evaluated using WinFit software (Novocontrol).

The size of micelles has been determined by dynamic light scattering (DLS) using a Zetasizer Nano-ZS (Malvern Instruments).

2.2. Preparation of aluminum chelate complex

The synthesis of Al (dips)$_3$ is outlined in detail elsewhere [23]. Briefly, 3,5-diisopropyl salicylic acid (96%, Acros Organics) is dissolved in dried methanol (⩾99.5% Ph. Eur., Roth) and given to a MeOH solution of an equimolar amount of $AlCl_3$ (99.99% metal basis, Sigma Aldrich) that contains the threefold molar concentration of sodium methoxide with respect to aluminum. This mixture is allowed to react for 30 min. Then the solvent is withdrawn by a rotary evaporator and the solid residue is dissolved in benzene. The benzene solution is stored in a refrigerator at about 8 °C in order to allow crystallization of formed NaCl. The supernatant is separated by decantation and the solvent again is withdrawn by rotary evaporation at reduced pressure. After recrystallization from diethyl ether, evaporation of this solvent and drying in fine vacuum the aluminum complex is obtained as a powder. The reaction product is readily soluble in hexadecane up to millimolal concentrations.

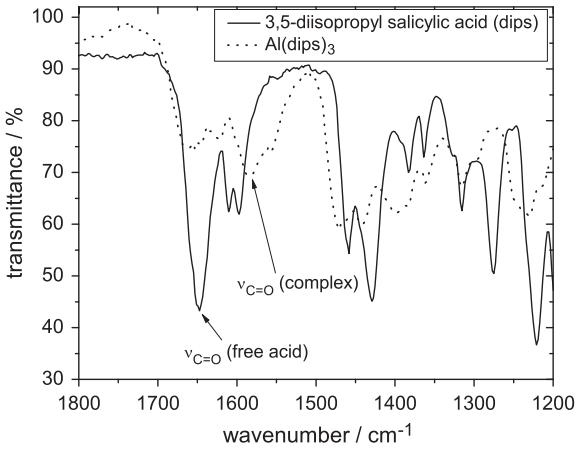

Fig. 1. IR spectra of 3,5-diisopropyl salicylic acid (dips) and the aluminum chelate complex Al (dips)$_3$.

Formation of the metal chelate compound has been proven by means of IR spectroscopy. IR spectra have been sampled using a Digilab FTS3100 FTIR spectrometer in ATR setup. A shift of $\nu_{C=O}$ of 3,5-diisoproyl salicylic acid from 1655 cm^{-1} (free acid) to 1580 cm^{-1} (chelate) is observed (Fig. 1). This shift to lower wave numbers due to chelate formation between metal ions and salicylic acid derivatives is due to a weakening of the C=O bond [24]. Moreover, the free acid is characterized by spectral bands at 1226 cm^{-1} and 1280 cm^{-1} [25]. These bands are not observed in the case of 3,5-diisopropyl salicylic acid acting as a complex ligand.

3. Results and discussion

3.1. DC conductivity in dependence on solute concentration

3.1.1. DC conductivity of AOT hexadecane solutions

Fig. 2 summarizes the dependence of low frequency conductivity of sodium AOT solutions on concentration determined by impedance analysis at 10^{-2} Hz. The magnitude of low frequency (complex) conductivity shown is mainly governed by the real part of conductivity and thus is a good approximation for DC conductivity.

As can be seen, conductivity σ (Fig. 2) in dependence on solute concentration c cannot be fully explained with well-known theories applicable to aqueous electrolytes. In the case of (complete) dissociation of a binary 1:1-electrolyte in water – which holds for small solute concentrations and small activities – the linear dependence of conductivity on the square root of solute concentration is well-known (Kohlrausch's law). A closer inspection of Fig. 2 reveals, however, that the graph may be divided into three sections: At low solute concentrations up to approximately 10^{-6} mol/kg the dependence of conductivity on concentration may be sufficiently explained by a dependence on the square root of the solute concentration ($\sigma \propto c^{1/2}$). A neutral solute NaAOT

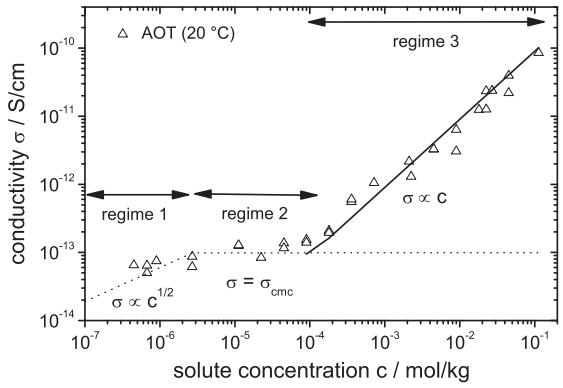

Fig. 2. DC conductivity in the system sodium AOT–hexadecane at 293 K.

molecule dissociates to form Na^+ and AOT^- ions as charge carriers (regime 2). In the concentration range 10^{-6} mol/kg to approximately 10^{-4} mol/kg a plateau conductivity is observed whereas there is a noticeable increase in conductivity for higher AOT concentrations. The plateau conductivity might be due to the (very small) dissociation constant of sodium AOT that limits the concentration of charge carriers present in the system (regime 2, $\sigma = \sigma_{cmc} = \text{constant}$). This behavior has been reported for the AOT dodecane system and may be readily understood [2,3]: formation of small charged species like Na^+ or AOT^- – despite of a hydration shell which will be present due to trace amounts of water dissolved in the hydrocarbon – is extremely unfavorable in nonpolar media from a thermodynamic point of view. The Bjerrum length l_b, the characteristic length where the Coulombic energy between two opposed point charges (of charge magnitude $1e$) is counterbalanced by thermal energy k_BT, accounts for this aspect:

$$l_b = \frac{e^2}{4\pi\varepsilon_0\varepsilon_r k_B T}, \tag{1}$$

with e: elementary charge, ε_0: vacuum permittivity, ε_r: relative permittivity, k_B: Boltzmann constant and T: temperature.

The Bjerrum length is inversely proportional to ϵ_r: in a nonpolar environment like hexadecane ($\varepsilon_r \approx 2$) l_b is about 28.0 nm (298 K) whereas in polar media like ethanol ($\varepsilon_r \approx 25$) and water ($\varepsilon_r \approx 81$) it is around 2.2 nm and 0.7 nm, respectively. Thus, the Bjerrum length in nonpolar environment like hexadecane is about 40 times larger than in water and charge recombination will occur if opposed charge carriers are not separated by l_b or a larger (center–center-) distance r. This has some important implications for nonpolar media:

- Only a minute number of charged species will be present, thus dissociation is unfavorable and the probability for ion formation is given by $\exp(-l_b/r)$.
- Formation of ionic species of high charge density is energetically unfavorable, i.e. highly charged ions will not exist.
- "Stable" charge carriers must exhibit a low charge density, i.e. they should be bulky "macro-ions" that carry a small charge ($|z| = 1$).

In nonpolar systems singly charged reverse AOT micelles have been reported to act as charge carriers [1]. The increase in conductivity for AOT concentrations of more than 10^{-4} mol/kg (see Fig. 2) may be explained by "macro-ions", i.e. charged micelles that are formed at high solute concentrations (regime 3). The cmc in nonpolar media is not a well-defined quantity but frequently a quite broad concentration range exists where a gradual formation of micelles starts. In the case of sodium AOT dissolved in hexadecane a cmc region in the concentration range 10^{-6} mol/kg to 10^{-4} mol/kg may be identified from conductivity data. Macro-ions will be the prevailing charge carriers for solute concentrations larger than cmc (regime 3). Charge transport in hydrocarbon systems under these conditions will be more effective compared to regime 1 where only a small number of "ions" due to dissociation of molecular compounds will be present.

3.1.2. DC conductivity of lecithin hexadecane and Al (dips)$_3$ hexadecane solutions

Lecithin shows a similar dependence of conductivity on solute concentration like AOT (see Fig. 3a). Again the course of conductivity over solute concentration may be divided into the aforementioned three regimes and a change in activation energy of conduction is observed, too (see Fig. 7). In the case of lecithin this behavior is expected since the molecular structure resembles an amphiphilic compound like AOT that forms micelles. The critical micelle concentration of lecithin is known to be 9×10^{-4} mol/kg in benzene for the formation of "large" micelles [26,27] but a cmc has been reported of about 4×10^{-6} mol/kg, too, for the formation of "small" micelles. The cmc of lecithin in hexadecane is expected to be in a comparable concentration range. The small micelles consist of 4–5 monomeric units of lecithin [28,29]. The size of reverse micelles formed in hydrocarbons is influenced by the amount of water present in the system: with minute amounts of water present depending on the micelle volume fraction spherical micelles of diameters between 4.8 nm and 10.8 nm have been determined by SANS in a cyclohexane–lecithin–water system [30]. Mackeben et al. [31] report spherical lecithin micelles sized 5–12 nm present in an isopropyl myristate–lecithin–timolol maleate system depending on water and timolol maleate content. At higher water content worm-like micelles have been observed [30,32]. DC conductivity of lecithin in hexadecane presented in Fig. 3 shows a plateau conductivity in the concentration range of about 5×10^{-6} mol/kg to 2×10^{-5} mol/kg,

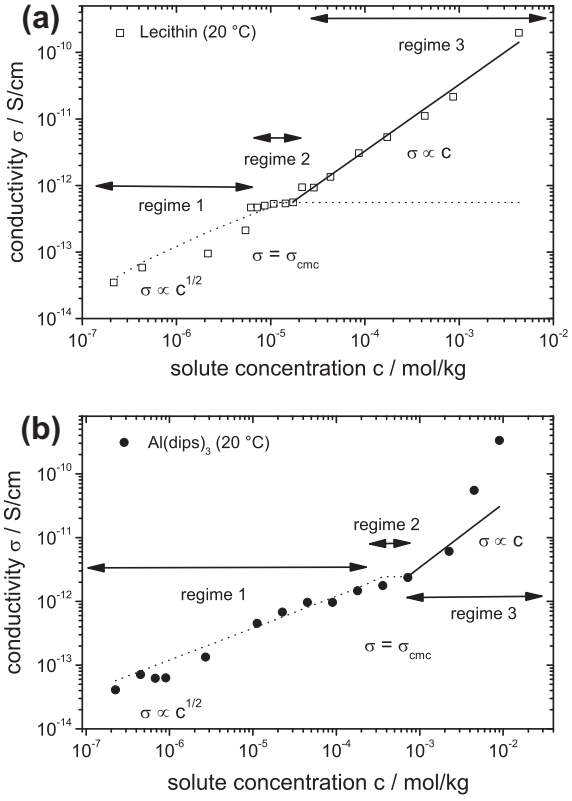

Fig. 3. (a) DC conductivity in the systems lecithin–hexadecane at 293 K. (b) Al (dips)$_3$–hexadecane at 293 K.

i.e. this is identified to be the cmc region. In the lecithin–hexadecane system there are only traces of water present. Therefore the micelles are assumed to be of spherical shape. A micelle size of 7.0 nm (hydrodynamic diameter) has been determined by DLS.

For Al $(dips)_3$ no formation of micellar structures can occur. The dependence of conductivity on concentration can be explained sufficiently by a dependence on the square root of the solute concentration for concentrations up to millimolal concentrations, i.e. the charged species are formed due to dissociation of the molecular compound. For higher concentrations deviations from this dependence are noticeable. Presumably the aluminum salicylate complex will form charged adduct species at higher solute concentrations that may act as charge carriers. A more complicated mechanism of charge carrier generation is obvious (deviation from $\sigma \propto c^{1/2}$ and $\sigma \propto c$).

3.2. Charge transport in nonpolar systems

From DC conductivity data one may conclude that charge transport in the systems studied is due to ionic conduction with a dependence $\sigma \propto c^{1/2}$ for charge carrier generation due to dissociation and $\sigma \propto c$ for micellar charge carriers. In this case the conductivity σ in solutions is related to ionic mobilities μ_i and to the concentration n_i of charged species i present in the system:

$$\sigma = \sum_i n_i |z_i| e \mu_i, \tag{2}$$

with μ_i: mobility of species i, n_i: concentration of species i, z_i: charge number of species i, and e: elementary charge.

For spherically shaped charged species the charge carrier mobility μ_j for species j may be related to the hydrodynamic radius R_j of ion j:

$$|z_j| e = 6\pi\eta R_j \mu_j, \tag{3}$$

with η: solvent viscosity.

The formation of charged micelles is claimed to be due to auto dissociation of two (neutral) micelles [1–3]. If one assumes micellar singly positively and negatively charged structures of same size and charge generation due to disproportionation of neutral micelles which is true in the case of AOT and lecithin it holds that

$$2M \rightarrow M^+ + M^-, \tag{4}$$

with M: micelle.

Under the aforementioned assumptions, i.e. $|z_i| = 1$ the total charge carrier number density $n_\pm$ in the concentration range where charged micelles are the predominant charge carrier species may be estimated from conductivity data [1]:

$$n_\pm = \frac{\sigma 6\pi\eta R_i}{e^2}. \tag{5}$$

Applying above mentioned simplifications e.g. the Debye length $1/\kappa$ in nonpolar systems may be calculated from Eq. (5) if the conductivity and the hydrodynamic radius of the charge carriers present are known:

$$\frac{1}{\kappa} = \sqrt{\frac{\varepsilon_r \varepsilon_0 k_B T}{6\pi\eta R_i \sigma}}. \tag{6}$$

The radius of sodium AOT reverse micelles in hydrocarbon media (dodecane) is 1.56 nm [2,33]. For lecithin reverse micelles a hydrodynamic diameter of 7.0 nm has been determined by DLS. Only negligible changes in micelle size are expected under the given experimental conditions [34,35]. Accordingly, the Debye lengths summarized in Fig. 4 are obtained assuming the above mentioned values for micelle size for AOT and lecithin and taking into account the material parameter of hexadecane. For Al $(dips)_3$ a radius of 0.8 nm has been estimated from complex constitution. The same value has been assumed for the radius of the positively charged counter ion. The Debye lengths obtained for these nonpolar systems are in the range of 10^{-7} m to several 10^{-6} m. In aqueous systems they are typically in the order of magnitude of nanometers. This implies that electrostatic interactions in nonpolar media – in contrast to aqueous systems – will be long-ranged due to low screening (small ε_r) and minute charge carrier concentrations (low σ). The equilibrium constant $K_{\text{eq,micelles}}$ for the disproportionation of micelles (see Eq. (4)) is given by

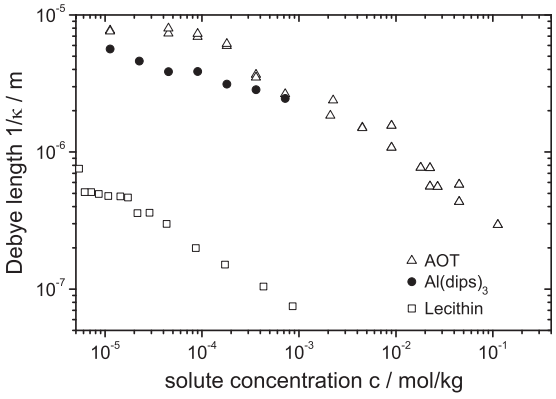

Fig. 4. Estimated Debye length $1/\kappa$ (see Eq. (6)) from DC conductivity in the micellar systems lecithin–hexadecane and sodium AOT–hexadecane and in the Al $(dips)_3$–hexadecane system (charge carrier generation due to dissociation) at 293 K.

$$K_{\text{eq,micelles}} = \frac{[M^+][M^-]}{[M]^2} = \frac{[M^\pm]^2}{[M_0 - M^\pm]^2} = \frac{\alpha^2}{(1-\alpha)^2}. \tag{7}$$

Activities are treated as concentrations for the sake of simplicity. The concentration of positively and negatively charged species M^+ and M^- is equal and may be expressed as $M^\pm$. If we introduce the total concentration of micelles in the system, M_0, the equilibrium constant may be expressed in terms of the degree of dissociation

$$\alpha = \frac{M^\pm}{M_0}, \qquad \alpha = \frac{\sqrt{K_{\text{eq,micelles}}}}{1 + \sqrt{K_{\text{eq,micelles}}}}. \tag{8}$$

A simple linear dependence of $M^\pm$ on the total solute concentration M_0 is obtained. As outlined Eq. (7) only holds for a charge carrier generation mechanism according to Eq. (4) that is not applicable to the aluminum complex. Al $(dips)_3$ is known to be a strong Lewis acid and Brønsted acid [23], i.e. charge carrier generation will be due to dissociation of the compound:

$$\text{Al (dips)}_3 + H_2O \leftrightarrow [\text{Al (dips)}_3^-] + [H_3O^+]. \tag{9}$$

In this case an equilibrium constant $K_{\text{eq,diss}}$ may be defined:

$$K_{\text{eq,diss}} = \frac{[H^+][\text{Al (dips)}_3^-]}{[\text{Al (dips)}]_3} = \frac{\alpha_{\text{diss}}^2}{1-\alpha_{\text{diss}}} c_0. \tag{10}$$

The H^+ ions might be transferred to water clusters within the organic solvent. According to Eq. (9) the total charge carrier concentration is expected to be proportional to the square root of the solute concentration. This is obviously the case: evaluation of DC conductivity data of the Al $(dips)_3$ hexadecane system (see Fig. 4) leads to a linear dependence of $\log(1/\kappa)$ over $\log(c(\text{Al(dips)}_3))$ with a slope

$$\frac{d\log(1/\kappa)}{d\log(c(\text{Al (dips)}_3))} \approx \frac{1}{2}\frac{d\log(1/\kappa)}{d\log(c(\text{AOT}))} = \frac{1}{2}\frac{d\log(1/\kappa)}{d\log(c(\text{lecithin}))}. \tag{11}$$

If we assume that charge carriers are of spherical shape and $|z_i| = 1$ and combine Eqs. (5) and (8) the following expression is obtained:

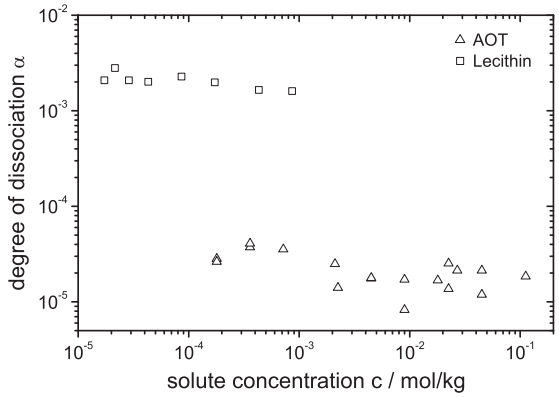

Fig. 5. Degree of dissociation α evaluated for AOT and lecithin micelles in hexadecane at 293 K.

$$\sigma = \frac{\alpha M_0 e^2}{6\pi\eta R_i}. \tag{12}$$

α and the equilibrium constant $K_{\text{eq,micelles}}$ may be estimated. For calculation of micelle number density it is assumed that the micelle density is equal to the solvent density and that the aggregation number is 30 for AOT and 18 for lecithin, respectively [17,30,31].

According to Fig. 5 only a minute fraction of micelles is charged. This result is expected because the formation of charged species is thermodynamically not favorable in nonpolar environment as outlined above. Obviously the micelle size does not depend on solute concentration: α is more or less constant over a wide concentration range although a slight decrease with increasing solute concentration might be noticed. The standard deviation of the degree of dissociation (for more or less constant values of α) may be used as an estimate of the error of this determination procedure. The mean value ($\pm$ standard deviation) of $\alpha = (2.2 \pm 0.9) \times 10^{-5}$ obtained for the AOT hexadecane system is somewhat larger than data reported for a NaAOT dodecane system ($\alpha = 1.5 \times 10^{-5}$) [2]. For lecithin $\alpha = (2.12 \pm 0.51) \times 10^{-3}$ is obtained. One might think of two possible reasons for the slightly decreasing degree of dissociation with increasing solute concentration: On the one hand the degree of dissociation is known to be a function of solute concentration and is only constant at small concentrations. It will decrease with increasing solute concentration. This is in accordance with the behavior observed. On the other hand a decreasing degree of dissociation with increasing solute concentration also might be due to an increasing mean size of micelles with increasing solute concentration. In this case one would notice an apparent decrease of the degree of dissociation with assuming a concentration independent micelle size.

3.3. Temperature dependence of conductivity and equivalent circuit representation for the lecithin hexadecane system

A change in charge carrier speciation in dependence on the total solute concentration c, i.e. ions vs. charged micelles in addition to the changes of the slope $d\sigma/dc$ can be identified by temperature dependent measurements of conductivity. Larger charged structures like micelles are more stable compared to small ions. Therefore a smaller activation energy for conduction in the micellar regime compared to the concentration range where ions act as charge carriers is expected. The activation energy that may be determined by temperature dependent conductivity measurements cannot be attributed to a single process but is a quantity being characteristic for the behavior of the whole system describing all processes taking place within the system. The fact that this activation energy cannot be solely attributed to the conduction but e.g.

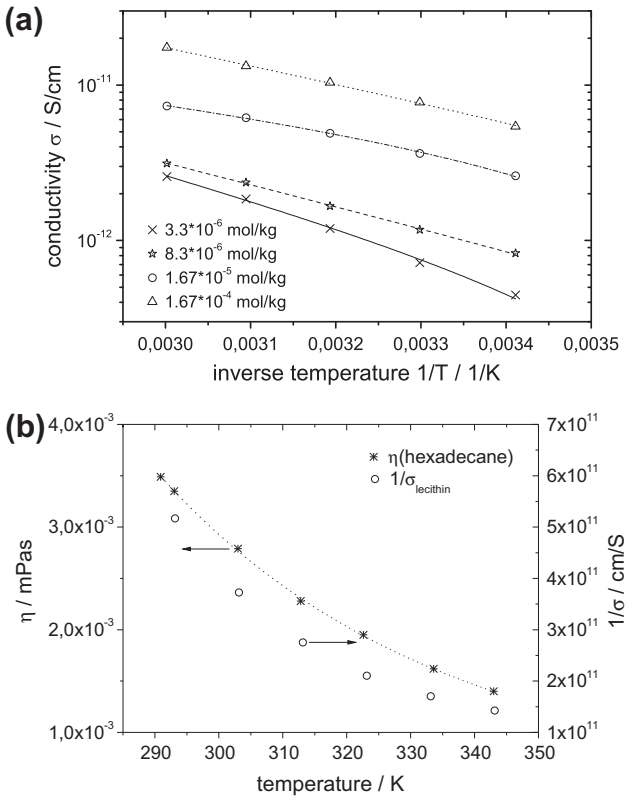

Fig. 6. (a) Arrhenius plot of DC conductivity (lecithin–hexadecane system) in dependence on temperature (symbols: experimental data; lines: fit function). (b) Temperature dependence of inverse conductivity $1/\sigma$ and solvent viscosity η.

also might imply some contributions from the micelle auto-dissociation equilibrium has been indicated by using the term "apparent activation energy of conduction". In Fig. 6a the Arrhenius plot for the determination of the apparent activation energy of conduction E_A is depicted exemplarily for lecithin systems of different solute concentration. The change of charge carrier regimes is noticeable (c.f. similar slopes for concentrations in the range where micelles are present, different slope for a solute concentration of 3.3×10^{-6} mol/kg where no micelles exist). Typical correlation coefficients between 0.997 and 0.999 are obtained. The activation energies obtained reflect different mechanisms influencing charge transport. First, with increasing temperature the charge carrier concentration is expected to increase due to shifted dissociation equilibria. Besides this change in the degree of dissociation with increasing temperature the solvent viscosity decreases which will lead to higher ion mobilities (see Eq. (3)). Besides a change in viscosity one also might think of a change of micelle size with temperature. However in the systems under consideration with small amounts of water only negligible changes of micelle radii in the temperature range studied are expected [35,34,36]. Saad et al. [35] studied the temperature and pressure dependence of AOT reverse micelle sizes in a n-heptane system that contained traces of water. They found a small decrease in micelle size from (1.54 ± 0.02) nm at 293 K to (1.45 ± 0.01) nm at 333 K (1 atm). Zulauf et al. [34] thoroughly characterized the ternary H_2O/AOT/isooctane system. In the presence of water exceeding the AOT amount by a factor of 10 or more a remarkable temperature dependence of micelle size has been reported (increase by a factor of 2 if the temperature is increased from 293 K to 333 K). A constant micelle size of (1.5 ± 0.3) nm has been found in isooctane that only contained trace amounts of water in the temperature range 293–368 K. A more or less constant micelle size as studied by SANS has been reported

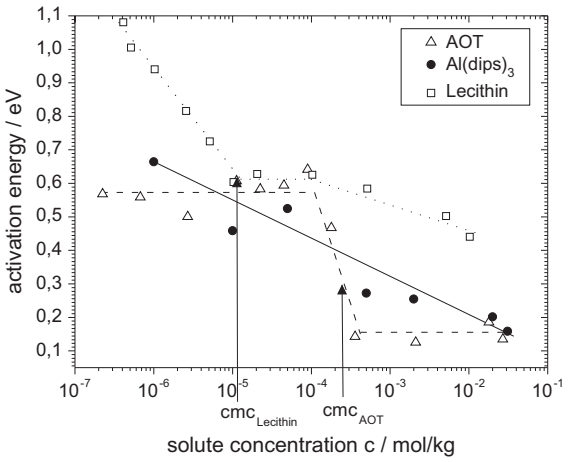

Fig. 7. Activation energy for conduction in dependence on solute concentration (sodium AOT: triangles, lecithin: open squares, Al $(dips)_3$: filled circles) determined by Arrhenius evaluation of conductivity data in the temperature range 293–333 K).

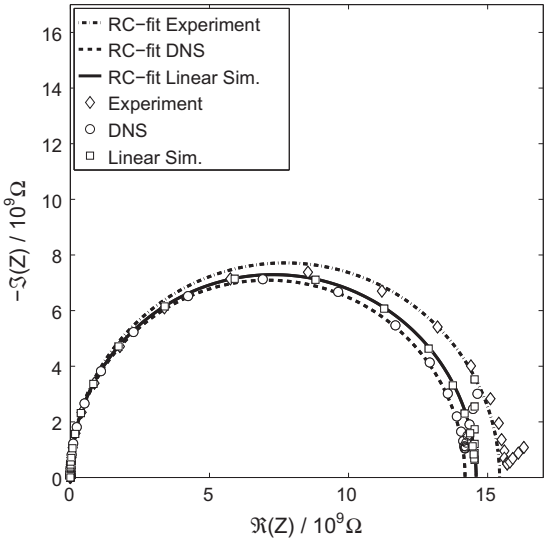

Fig. 8. Cole–Cole plot of experimental and simulated impedance data (direct numerical simulation (DNS) and linear simulation) and their corresponding RC fits, see (14), of a lecithin hexadecane solution (c(Lecithin) $= 1.67 \times 10^{-4}$ mol/kg, $T = 293$ K).

for mixed reverse micelles consisting of AOT and lecithin in the temperature range 293–343 K, too [36]. Thus, we conclude that in the hexadecane systems under consideration being comparable to these systems the increase in conductivity with temperature is mainly due to changes in solvent viscosity and not micelle size. Fig. 6b supports this interpretation. The inverse conductivity $1/\sigma$ and the solvent viscosity η in dependence of the temperature are shown. Both quantities decay exponentially with increasing temperature.

In Fig. 7 the apparent activation energy of conduction E_A obtained by Arrhenius evaluation (see Eq. (13)) of the DC conductivity σ in the temperature range 293–333 K for different solute concentrations of AOT, Al $(dips)_3$ and lecithin is summarized.

$$\ln(\sigma) = \ln(\sigma_0) - \frac{E_A}{k_B T}, \tag{13}$$

with σ: conductivity, E_A: activation energy, k_B: Boltzmann constant and T: temperature.

Two distinct regions can be identified with respect to the dependence of the activation energy on the solute concentration (Fig. 7): with ions present as charge carriers i.e. in the case of small concentrations of AOT sodium salt the activation energy for conduction is 0.5–0.6 eV whereas at higher concentrations of AOT where micellization occurs an activation barrier of about 0.15–0.2 eV is found. A very sharp decrease in the activation energy is observed near the cmc. In the case of lecithin we observe a higher activation barrier at smaller solute concentrations, too. At micellization a decrease in activation energy from 1.0–1.1 eV to 0.5–0.6 eV is quantified. In the Al $(dips)_3$ hexadecane system a change in activation energy from about 0.6 eV to 0.3–0.2 eV occurs for solute concentrations of about more than 10^{-4} mol/kg, i.e. here the transition from small ions as charge carriers to larger charge carriers like charged dimers is more gradual. The change in the activation energy presented in Fig. 7 and the change of the slopes of DC conductivity in dependence on solute concentration occurring near the cmc (see Figs. 2 and 3) agree fairly well.

3.4. Equivalent circuit representation for the lecithin hexadecane system

The fact that doped nonpolar systems exhibit ionic conduction may be noticed in equivalent circuit representations of impedance data, too. Fig. 8 shows a Cole–Cole plot, i.e. the representation of the negative imaginary part of complex impedance $-\Im(Z)$ over the real part $\Re(Z)$ for the lecithin hexadecane system studied at 293 K for a solute concentration of 1.67×10^{-4} mol/kg. Experimental impedance data as well as simulated impedance data using a direct numerical simulation (DNS) approach and a linear model show a semicircular feature followed by a straight line. Thus, the bulk impedance behavior of the micellar solutions approximately can be described by a simple RC circuit ($R||C$) in the equivalent circuit representation, i.e. using a Ohmic resistance R and a capacitance C. In this case the impedance $Z_{RC}(\omega)$ is given by

$$\frac{1}{Z_{RC}(\omega)} = \frac{1}{R} + \imath\omega C. \tag{14}$$

The characteristic conductivity relaxation times $\tau = RC$ obtained for the different equivalent circuit representations are comparable and typically in the order of magnitude of some 10 ms to seconds and show a dependence on solute concentration and temperature. Inverse relaxation times are linearly increasing with increasing solute concentration which is in accordance with an ionic conduction mechanism.

The values for capacity and resistance obtained from the numerical simulations are smaller than the values fitted from experimental data (see Table 1). The reason can be found in the deviations shown in Figs. 10 and 11. For an explanation see Section 7.

4. Poisson–Nernst–Planck–Stokes model

Nernst–Planck is the model of choice if one considers ion transport in dilute solutions. A key assumption is that one can neglect interactions between individual ions. Therefore the PNP equations

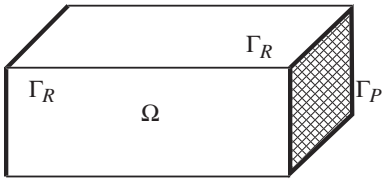

Fig. 9. Schematic view of the fluid region Ω. The conducting surfaces Γ_P are on the left an right side. The symmetry boundaries are marked as Γ_R.

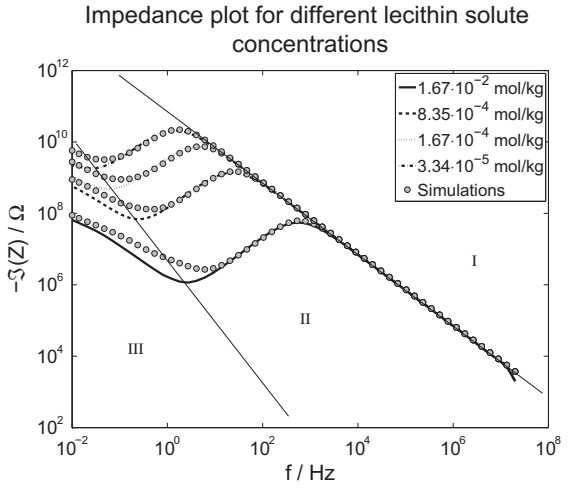

Fig. 10. Comparison of measured impedance with results from the DNS.

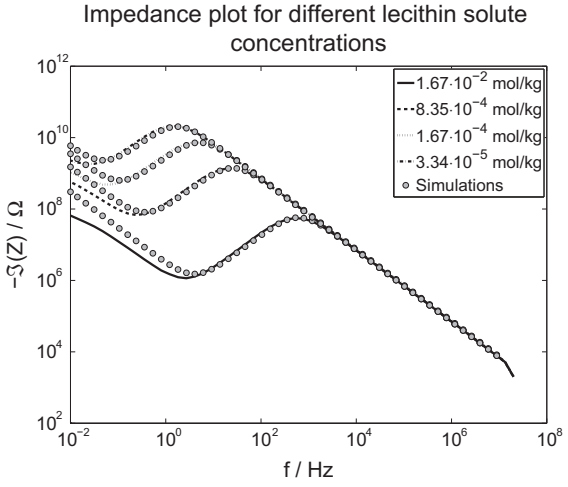

Fig. 11. Comparison of measured impedance with results from linear simulations.

provide a mechanism to describe the response to an applied voltage. For large frequencies the perturbation of the static equilibrium $n_+ = n_- = N, N$ being the concentration of dissociated ions, is small and the PNP approach is valid. We use this to determine the concentration of dissociated ions. In the next subsection we formulate the theoretical model. Starting from this model two numerical methods (direct numerical simulation (DNS) and linear simulation) are presented in Sections 6 and 5. With these methods we are able to compare the experimental results with the theoretical PNPS model (see Section 7).

4.1. Formulation of the theoretical model

For our theoretical model we begin with the time-dependent Poisson–Nernst–Planck–Stokes system, see [37]. For a nonpolar liquid containing a number #Species of different ionic species the describing equations are

$$-\nabla\cdot(\varepsilon_0\varepsilon_r\nabla\varphi) = \sum_{s=1}^{\#\text{Species}} ez_s n_s, \quad \text{Poisson} \tag{15a}$$

$$\partial_t n_s + \nabla\cdot\mathbf{J}_s = 0, \quad \text{Nernst—Planck} \tag{15b}$$

$$\rho\partial_t\mathbf{u} - \nabla\cdot\left(-p\mathbb{I} + \mu(\nabla\mathbf{u} + \nabla\mathbf{u}^\top)\right) = -\sum_{s=1}^{\#\text{Species}} ez_s n_s\nabla\varphi, \quad \text{Momentum} \tag{15c}$$

$$\nabla\cdot\mathbf{u} = 0. \quad \text{Continuity} \tag{15d}$$

See Fig. 9 for a schematic view of the domain of interest.

For this system of nonlinear coupled partial differential equations with the electric potential φ, ion density n_s of species $s \in \{1,\dots,\#\text{Species}\}$, liquid velocity $\mathbf{u}$ and pressure p, we define the ion fluxes $\mathbf{J}_s$ by

$$\mathbf{J}_s = -n_s\left(\frac{D_s}{k_BT}\nabla\mu_s - \mathbf{u}\right), \tag{15e}$$

$$\mu_s = k_BT\ln n_s + ez_s\varphi, \tag{15f}$$

with diffusion constant D_s, Boltzmann constant k_B, specific charge ez_s and temperature T. On the boundary the velocity is set zero. The conducting surfaces Γ_P are completely blocking (no ion transfer), i.e. we have the following boundary conditions

$$\varphi = U_p(t) = U_c\Re e^{i\omega t}, \quad \partial_\nu\mu_s = 0, \tag{15g}$$

where U_c is a different constant on each of the conducting surfaces of the capacitor. At the remaining part of the boundary Γ_R we use symmetry conditions

$$\partial_\nu n_s = 0, \quad \partial_\nu\varphi = 0, \tag{15h}$$

which leads to conservation of ion number. Using this model we compute the impedance–frequency response defined as the

Table 1
(a) Evaluation of impedance data for a lecithin hexadecane system (293 K) using the $R\|C$ equivalent circuit representation. (b) Fitted values of experimental and simulated impedance data of a lecithin hexadecane solution (c(Lecithin) = 1.67×10^{-4} mol/kg, T = 293 K).

c (mol/kg)	R (Ω)	Err R (%)	C (F)	Err C (%)	τ (s)
(a)					
3.33×10^{-5}	6.65×10^{10}	0.47	2.33×10^{-12}	1.69	1.55×10^{-1}
1.67×10^{-5}	1.26×10^{11}	0.32	2.35×10^{-12}	2.06	2.97×10^{-1}
8.3×10^{-6}	2.03×10^{11}	0.45	2.36×10^{-12}	1.72	4.79×10^{-1}
3.3×10^{-6}	4.02×10^{11}	0.37	2.32×10^{-12}	1.59	9.31×10^{-1}
1.6×10^{-6}	7.29×10^{11}	0.56	2.23×10^{-12}	1.64	1.63
	R (Ω)	C (F)	τ (s)		
(b)					
Experiment	1.5429×10^{10}	2.2569×10^{-12}	3.48×10^{-2}		
DNS	1.4186×10^{10}	2.1287×10^{-12}	3.02×10^{-2}		
Linear Sim.	1.4586×10^{10}	2.1666×10^{-12}	3.16×10^{-2}		

quotient $Z_p(\omega) = U_p(t)/I_p(t)$ of the applied voltage and the electrical current. This concept only makes sense if $I_p(t)$ depends linearly on U_p. Note that by virtue of Gauss' Theorem the electric current is given by $I_p(t) = \varepsilon_0\varepsilon_r A\frac{d}{dt}\partial_\nu\varphi(t,0)$.

4.2. Non-dimensionalization of parallel plate capacitor with two species

For the purpose of simplicity let us study the planar plate capacitor, for which the solution of the system above has a translational invariance and hence no flow occurs, i.e. $\mathbf{u} \equiv \mathbf{0}$.

If boundary effects at Γ_R are neglected we can consider a $1D$ parallel plate capacitor geometry $\Omega = [0, x_c]$ instead of the full geometry. It is understood that the capacitor extends in the remaining two spatial dimensions, so that each plate has an area A. We nondimensionalize using the characteristic values

$$[x] = x_c, \quad [n_\pm] = n_c, \quad [\varphi] = U_c, \quad [t] = t_c,$$

which gives the nondimensional problem

$$-\Delta\varphi = R^c(z_+ n_+ + z_- n_-), \tag{16a}$$

$$\partial_t n_\pm = S^c_\pm \Delta n_\pm \pm Z K^c_\pm \nabla\cdot(n_\pm\nabla\varphi), \tag{16b}$$

where

$$R^c = \frac{x_c^2 e n_c}{\varepsilon_0\varepsilon_r U_c}, \qquad S^c_\pm = \frac{t_c D_\pm}{x_c^2}, \qquad K^c_\pm = \frac{t_c D_\pm e U_c}{k_B T x_c^2}. \tag{17}$$

so that the total ion content

$$N_\pm = \int_0^1 n_\pm(t,x)dx > 0.$$

is conserved and the total charge vanishes, i.e. $N_+z_+ + N_-z_- = 0$. Now we want to find solutions of Eq. (16) which converge to $(2\pi/\omega)$-periodic functions, i.e. $\|n_\pm(t,\cdot) - n_\pm(t+2\pi/\omega,\cdot)\| \to 0$ and $\|\varphi(t,\cdot) - \varphi(t+2\pi/\omega,\cdot)\| \to 0$ as $t\to\infty$. This will generally result in a nonlinear problem.

A linear dependence between U_p and I_p can only be expected if the applied voltage U_p is sufficiently small. Therefore assume $\varphi = \delta\widehat{U}e^{\imath\omega t}$ on the boundary with $\delta \ll 1$ and proceed as follows.

5. Linear response to small voltages

The approximate problem can be dealt with much more efficiently, but note that its validity may be restricted to small values of δ. For the moment we assume that the time-periodic responses of the electric potential φ and deviations of the ion density are (affine) linear in the applied periodic input $U_p(t)$ and therefore that the solution of the PNP Eq. (16) can be expanded as

$$n_\pm(t,x) = n^0_\pm(x) + \delta n^1_\pm(x)e^{\imath\omega t} + e^{2\imath\omega t}O(\delta^2),$$
$$\varphi(t,x) = \varphi^0(x) + \delta\varphi^1(x)e^{\imath\omega t} + e^{2\imath\omega t}O(\delta^2),$$

where the coefficients decay sufficiently fast.

Leading order problem $\mathcal{O}(\delta^0)$. Substitution of the above relation into the PNP equations and expanding with respect to δ we obtain to leading order

$$-\Delta\varphi^0 = R^c(z_+ n^0_+ + z_- n^0_-),$$
$$0 = S^c_\pm\Delta n_\pm \pm Z K^c_\pm\nabla\cdot(n_\pm\nabla\varphi),$$

with boundary conditions $\varphi^0(0) = \varphi^0(1) = 0$ and $\partial_\nu\mu^0_\pm(0) = \partial_\nu\mu^0_\pm(1) = 0$. Furthermore we have conservation of ion content

$$\int_0^1 n^0_\pm(x)\mathrm{d}x = N_\pm.$$

The solution to this leading order equation is given by $n^0_\pm(x) = N_\pm$ and $\varphi^0(x) = 0$.

Next order correction $\mathcal{O}(\delta^1)$: Computing the terms at next order we obtain

$$-\Delta\varphi^1 = R^c(z_+ n^1_+ + z_- n^1_-), \tag{18a}$$

$$\imath\omega n^1_\pm = S^c_\pm\Delta n^1_\pm + z_\pm K^c_\pm N_\pm\Delta\varphi^1, \tag{18b}$$

with boundary conditions $\varphi^1(0) = 0, \varphi^1(1) = \widehat{U}$ and Neumann conditions $\partial_\nu\mu^0_\pm(0) = \partial_\nu\mu^0_\pm(1) = 0$. Here, we have used $\varphi^0 \equiv 0$ from the leading order computation. Since the ion content is fixed by the leading order relation we need to impose

$$\int_0^1 n^1_\pm(x)\mathrm{d}x = 0.$$

Using Gauss's law and the definitions above yields

$$U_p(t) = \delta U_c e^{\imath\omega t}\widehat{U}(0), \tag{19}$$

$$I_p(t) = \delta U_c e^{\imath\omega t}(\imath\omega\varepsilon_0\varepsilon_r A/x_c)\partial_\nu\varphi^1(0) + \mathcal{O}(\delta^2), \tag{20}$$

where ∂_ν is the derivative in normal direction. Therefore the impedance is

$$Z_p(f) = \frac{\widehat{U}(0)x_c}{\imath\omega\varepsilon_0\varepsilon_r A\partial_\nu\varphi^1(0)}. \tag{21}$$

In terms of a discretized weak formulation the $\mathcal{O}(\delta)$ problem for φ^1 and $n^1_\pm$ with frequency $\omega = 2\pi f$ amounts to solving

$$\begin{pmatrix} \mathbf{S} & -R^c z_+\mathbf{M} & -R^c z_-\mathbf{M} & \mathbf{B}_1^\top \\ z_+K^c_+N_+\mathbf{S} & \imath\omega\mathbf{M} + S^c_+\mathbf{S} & 0 & \mathbf{B}_2^\top \\ z_-K^c_-N_-\mathbf{S} & 0 & \imath\omega\mathbf{M} + S^c_-\mathbf{S} & \mathbf{B}_3^\top \\ \mathbf{B}_1 & \mathbf{B}_2 & \mathbf{B}_3 & 0 \end{pmatrix}\begin{pmatrix}\varphi^1\\ n^1_+\\ n^1_-\\ \lambda\end{pmatrix} = \begin{pmatrix}0\\0\\0\\b\end{pmatrix}, \tag{22}$$

with standard mass matrix $\mathbf{M}$ and stiffness matrix $\mathbf{S}$. For a more detailed definition see Eq. (27) in the numerics section. The matrices $\mathbf{B}_1, \mathbf{B}_2, \mathbf{B}_3$ and vector λ account for the Dirichlet conditions for $\varphi^1, \varphi^1(0) = 0$ and $\varphi^1(1) = 1$, and the ion content $N_\pm$ conservation, respectively, and b the corresponding right hand side.

Obviously, the formulation (22) is immediately valid in any number of spatial dimension or in complex geometries, except for the definition of the electric current

$$I_p(t) = \frac{d}{dt}\int_\Gamma \varepsilon_0\varepsilon_r\partial_\nu\varphi(t,x)dA,$$

where Γ is the conducting surface of the capacitor, from or to which we want to measure the electric current.

Now for any given value ω the impedance $Z(\omega)$ can be computed by solving Eq. (22) once.

In contrast to Brumleve et al. [19] who compute solutions of the fully nonlinear system (of which they perform a Fourier transformation for a small input-response to obtain the impedance spectrum), we directly extract the impedance data for any given frequency in one single step. In that respect our approach is similar to the theory developed by Franceschetti et al. [38].

Eq. (22) requires the solution of a sparse linear equation once. The finite element formulation has the advantage of being flexible in complex domains in spatial higher dimensions and the no-flux boundary condition is implemented in a natural way. The advantage of their finite volume type method is that they can easier account for the singular case, i.e. convection dominated problems and strong electric fields [38].

6. Direct numerical solution

Compared to the approach in the previous section, the calculation of the impedance response by solving the full system is much more involved. The results obtained by direct numerical simulations (DNS) are, however, valid in all regimes, not only in the linear response regime. Additionally, the DNS offers more insight into different mechanisms of the impedance response of the system.

6.1. Method

We consider the same dimensionless form of the PNP system as before for Eqs. (16a) and (16b). This allows us to use different mobilities and charge numbers without having different time scales for each ion species.

$$-\Delta\varphi - R^c\sum_s z_s n_s = 0, \tag{23}$$

$$\partial_t n_s - S_s^c\Delta n_s - K_s^c z_s\nabla\cdot(n_s\nabla\varphi) = 0, \quad s = 1,\dots,\#\text{Species}. \tag{24}$$

The choice

$$x_c = \sqrt{\frac{\varepsilon_0\varepsilon_r k_B T}{e^2 n_c}}, \quad t_c = \frac{x_c^2}{D}, \quad U_c = \frac{k_B T}{e}, \tag{25}$$

leads to the usual dimensionless formulation with $R^c = 1, S^c = 1$ and $K^c = 1$. The system 23,24 constitutes a *differential algebraic equation* (DAE) of index 1. This means that the first time derivative of the Poisson equation can be transformed into an explicit expression for $\partial_t\varphi$. The sometimes ignored fact about DAE is that *order reduction* may occur, when higher order time stepping methods are used for time discretization of this nonlinear system, see [39–42]. A time discretization which does not suffer from order reduction in the case of a DAE of index 1 is called algebraically stable.

Since the above system is also stiff, an A- or L-stable (implicit) scheme is required. In order to avoid unnecessarily small time steps because of possible oscillations, an L-stable scheme is preferable.

Splitting the system into two linear ones seems appealing at first sight. However, while this idea works very well for small ion concentration, where the coupling between the Poisson and Nernst–Planck equation is weak, for higher concentration a very small time step is required to get a stable solution. Therefore we solve the fully coupled problem.

For sufficient accuracy, the time discretization scheme should be of second order. There are only two feasible schemes known, which fulfill the requirements stated above. The first one is BDF2 [43], a multistep method. The second one, called DIRK (2,2) [44] is a diagonally implicit Runge–Kutta method. The BDF2 method requires only one nonlinear solve in each time step, whereas the specific Runge–Kutta method requires two nonlinear solves. For this reason, we selected BDF2 as our algorithm of choice. Note that BDF2 needs two previous time steps. To start the simulation one can calculate the first time step with a one step method, or assume to start the simulation at rest. In this case the values at time $t^{-1} = -\tau$ are the same at time $t^0 = 0$.

Linear finite elements are used for space discretization. Compared to finite differences, finite elements allow for a more natural way to incorporate the flux boundary condition Eq. (15h) and the possibility to use local grid adaptivity in an easy way. In our case, adaptivity is mandatory to resolve the boundary layers. Compared to existing computational work on PNP system, see [18–22], our approach differs in the way that we combine finite elements with a higher order time discretization scheme that is free from order reduction.

After time and space discretization, a nonlinear system has to be solved in each time step. We apply Newton's method. In practice three to four iterations are sufficient in every time step. The iteration matrix of the method is (example for two species)

$$J_F(\varphi,n_1,n_2) = \begin{bmatrix} S & -R^c z_1 M & -R^c z_2 M \\ \gamma K_1^c z_1 S[n_1] & M+\gamma(S_1^c S + K_1^c z_1 K[\nabla\varphi]) & 0 \\ \gamma K_2^c z_2 S[n_2] & 0 & M+\gamma(S_2^c S + K_2^c z_2 K[\nabla\varphi]) \end{bmatrix}, \tag{26}$$

with $\gamma = \frac{2}{3}\tau$ and τ the time step size. The four different submatrices resulting from the finite element space discretization are

$$M_{i,j} := (\phi_j,\phi_i), \quad S_{i,j} := (\nabla\phi_j,\nabla\phi_i), \tag{27a}$$

$$K[\nabla\varphi]_{i,j} := (\nabla\varphi\phi_j,\nabla\phi_i), \quad S[n]_{i,j} := (n\nabla\phi_j,\nabla\phi_i), \tag{27b}$$

where M is the standard mass matrix and S the standard stiffness matrix. The two other matrices are a weighted convection matrix and a weighted stiffness matrix. ϕ_i are the linear finite element basis functions and $(\cdot,\cdot)$ is the standard L^2 inner product.

With the solutions given at time t^k and t^{k-1} the solution at time t^{k+1} is calculated by the following procedure.

- Set $\phi^{k,0} = \phi^k, n_1^{k,0} = n_1^k$ and $n_2^{k,0} = n_2^k$.
- Solve

$$J_F\left(\varphi^{k,n}, n_1^{k,n}, n_2^{k,n}\right)\begin{bmatrix}\varphi^{k,n+1}\\ n_1^{k,n+1}\\ n_2^{k,n+1}\end{bmatrix} = -F\left(\varphi^{k,n}, n_1^{k,n}, n_2^{k,n}\right), \tag{28}$$

until

$$F\left(\varphi^{k,n+1}, n_1^{k,n+1}, n_2^{k,n+1}\right) \leqslant tol. \tag{29}$$

- Set $\phi^{k+1} = \phi^{k,n+1}, n_1^{k+1} = n_1^{k,n+1}$ and $n_1^{k+1} = n_1^{k,n+1}$.

The function F is defined by

$$F(\varphi,n_1,n_2) := \begin{bmatrix} 0 \\ M\left(\frac{1}{3}n_1^{k-1} - \frac{4}{3}n_1^k\right) - \gamma K_1^c z_1 S[n_1]\varphi \\ M\left(\frac{1}{3}n_2^{k-1} - \frac{4}{3}n_2^k\right) - \gamma K_2^c z_2 S[n_2]\varphi \end{bmatrix}. \tag{30}$$

This procedure has been implemented in **MATLAB**, where matrix structures and direct solvers are ready to use.

7. Numerical results

The aim of the simulations is to give a better estimate for the degree of dissociation α. For this purpose impedance results from the simulations are matched with impedance results from the experiments by varying the degree of dissociation. The complex impedance is evaluated in the following way. The voltage on the right capacitor plate is given by

$$U_p = \widehat{U}\left(e^{\imath 2\pi f}\right). \tag{31}$$

The electric field on the capacitor plate is assumed to have the form

$$E_p = \widehat{E}\Im\left(e^{\imath 2\pi f - \imath\phi}\right), \tag{32}$$

where ϕ is the phase shift. This assumption is valid for a wide area of high frequencies. With this and Gauss' law the electric current from/to the capacitor is

$$I_p = \varepsilon_r\varepsilon_0 A\dot{E} = 2\pi f\varepsilon_r\varepsilon_0 A\widehat{E}\left(e^{\imath 2\pi f - \imath\phi}\right), \tag{33}$$

where A is the area of the capacitor. Finally, the complex impedance is

Table 2
Input parameters for the simulations.

η (N s/m^2)	D (m^2/s)	A (m^2)	ε_r (1)	T (K)
2.780×10^{-3}	2.206×10^{-11}	3.612×10^{-4}	2.046	293

$$Z_p(f) = \frac{U_p}{I_p} = \frac{\hat{U}e^{i\phi}}{2\pi f \varepsilon_r \varepsilon_0 A \hat{E}}. \tag{34}$$

For the evaluation of Z_p the phase shift ϕ and the amplitude $\hat{E}$ are evaluated from the electric field data, given by $E = -\nabla\varphi$. To find the best approximation of the simulations to the real experiments the functional

$$\nu(\alpha) = \sum_{f \in \text{Frequencies}} \left(Z_p(f,\alpha) - Z_E(f)\right)^2 \tag{35}$$

is minimized using a derivate free minimization algorithm (fminbnd). Here, the degree of dissociation α is the dependent variable in the functional.

The geometric extension of the capacitor is taken from the cylindric sample cell (BDS1307, Novocontrol) mentioned in Section 2.1. The cell consists of an inner stainless steel cylinder of an outer diameter of 19.5 mm that is surrounded by a hollow stainless steel cylinder of an inner diameter of 26.5 mm, i.e. the distance between the electrode surfaces is 3.5 mm. The total effective height of the electrodes is 5 mm. Symmetry is assumed in z and azimuthal direction. Since the curvature of the device is small, a purely 1d simulation is justified.

The diffusion coefficient D is calculated from the Stokes–Einstein equation

$$D = \frac{k_B T}{6\pi\eta R}, \tag{36}$$

where η is the dynamic viscosity of hexadecane and R the hydrodynamic radius determined by DLS from Section 3.1.2.

For very small frequencies the capacitor is fully charged and discharged in each period. This contradicts the assumption made in Eq. (32). For that reason not all frequencies are considered in the minimization process. The parameters used in the simulation are displayed in Table 2. The results of the simulations for the lecithin system are printed in Table 3. These are similar to the results in the experimental chapter, see Fig. 5. The impedance data are given in Fig. 10. In the low frequency regime the curves do not fit due to the reasons stated above. We could have obtained much better agreement with the experimental result if we had increased the micelle diameter by a factor of 4–5. However, we were not able to find any justification in literature for these diameters. In this case the linear simulation seems to fit better with the experimental curve as its minimum reaches the minimum of the experimental curve. In contrast, the asymptotic behavior for low frequencies is better matched by the direct numerical simulation.

Three different regimes of impedance behavior can be observed in the simulations. These regimes are marked in Fig. 10.

I *Polarization*: The micelle concentration changes only locally near the capacitor plates. The area where these small changes occur are in the range of a 1–2 Debye lengths. There is no noticeable influence on the electric potential. The electric field response is in phase with the applied voltage. See Fig. 12 or Animation I in the online version.

Table 3
Optimal values for the degree of dissociation α obtained by comparing the experimental results with the simulations.

Lecithin solute conc. n (mol/kg)	1.67×10^{-2}	8.35×10^{-4}	1.67×10^{-4}	3.34×10^{-5}
Degree of dissociation α (1)	0.554×10^{-3}	0.463×10^{-3}	0.461×10^{-3}	0.783×10^{-3}

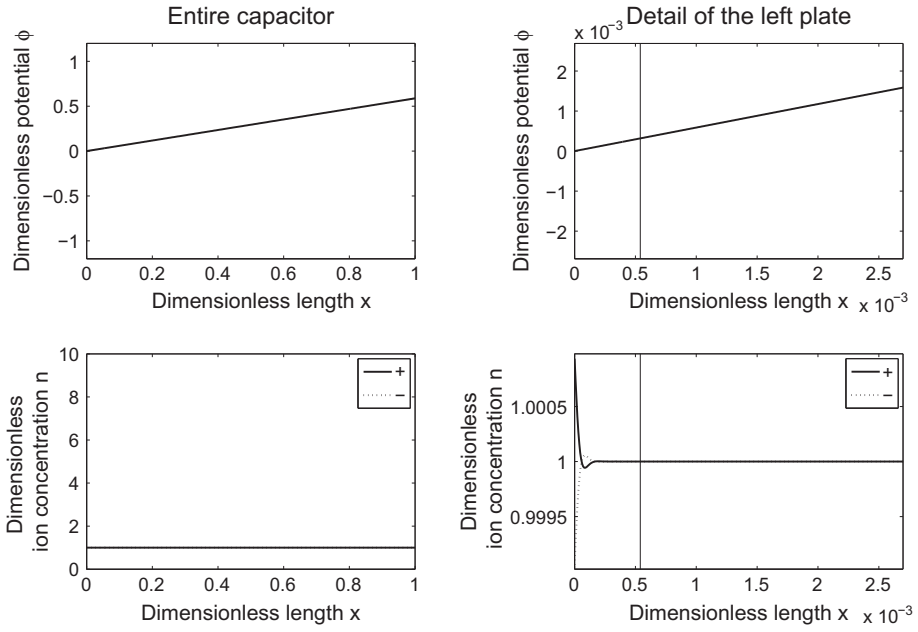

Fig. 12. Characteristic results for regime I: the variation of the ion concentration is very small. There is no deviation of the electric potential. The straight line in the detailed plots on the right indicate the Debye length.

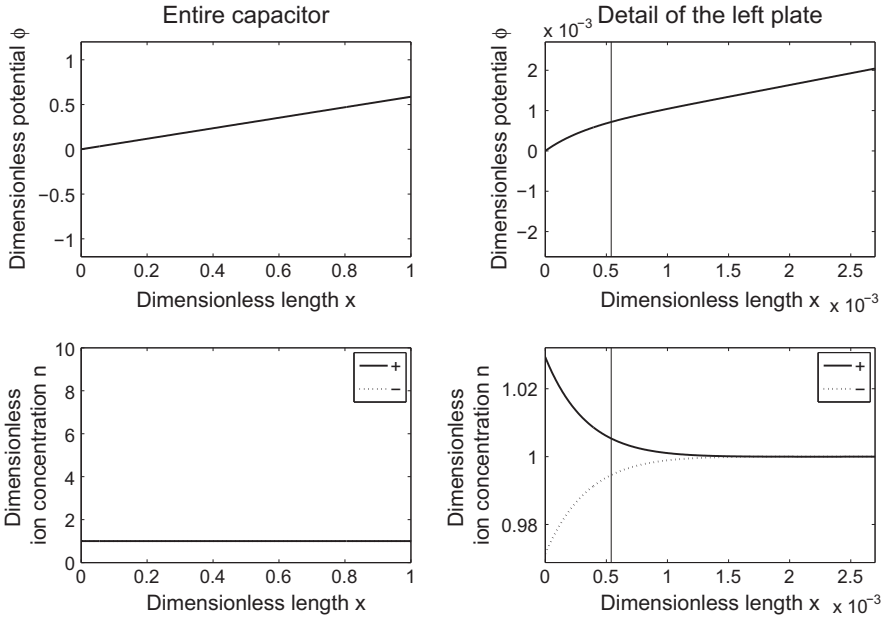

Fig. 13. Characteristic results for regime II: the variation of the ion concentration is still symmetric and small. The difference to regime I is the influence on the electric potential and a phase change. The straight line in the detailed plots on the right indicate the Debye length.

II *Mixed*: The ion transport still occurs in the small range of a few Debye lengths. In this area the electric potential is influenced by the ion concentration. The gradients become steeper. Also a phase shift can be observed between the applied voltage and the ion concentration due to the inertia of the lecithin micelles. The distributions of the positively and negatively charged ions remain symmetric on each plate. See Fig. 13 or Animation II in the online version.

III *Exponential layers*: In this regime huge exponential layers start developing on the capacitor plate. The local concentration is about 1000 times larger than the equilibrium concentration. The size of the layer is still in the scale of a few Debye lengths. The distributions of positively and negatively charged ions are unsymmetrical. A small part of the electric potential is blocked – the maximum gradient inside the capacitor is reduced. The change in phase is maximized. See Fig. 14 or Animation III in the online version.

Regimes I and II can be considered as linear. The Poisson equation and the Nernst–Planck equation are only weakly coupled in these regimes. Thus, the linear approximation returns good results compared to the DNS, but fails to catch the nonlinearities of regime III (see the asymptotic behavior for low frequencies in Figs. 10 and 11 or the right side of the Cole–Cole plot in Fig. 8).

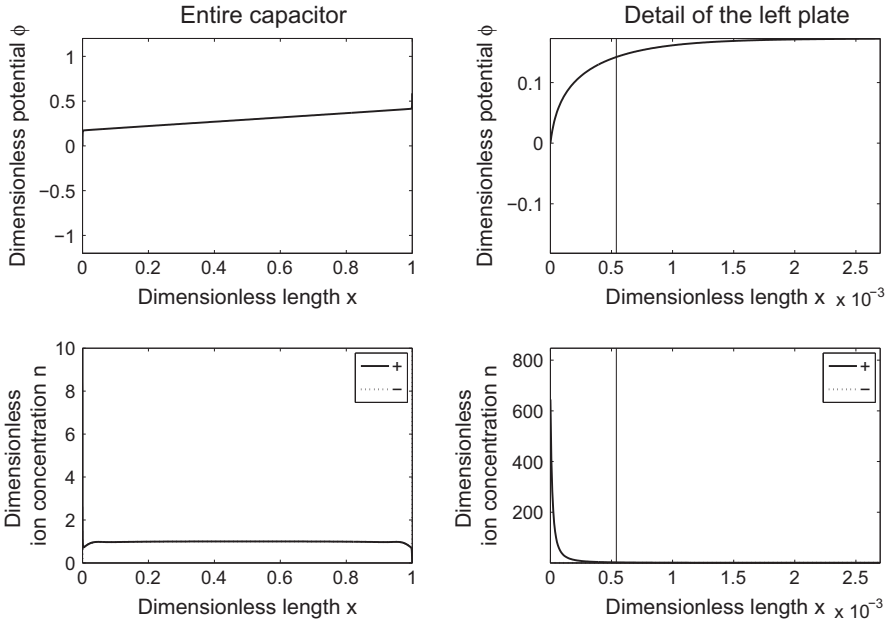

Fig. 14. Characteristic results for regime III: the ion concentration shows a pronounced exponential layer. The influence on the electric potential is huge. Its gradient inside the capacitor is smaller. The straight line in the detailed plots on the right indicate the Debye length.

8. Conclusions

Impedance measurements have been performed to characterize charge transport in doped hydrocarbon systems. A purely ionic charge transport mechanism has been identified. DC conductivities of systems forming reverse micelles, i.e. hexadecane solutions of sodium AOT and lecithin have been compared to conductivities of an aluminum chelate compound (Al (dips)$_3$). In the micellar systems for minute solute concentrations conductivity is dependent on the square root of the solute concentration, i.e. charge carriers are formed by dissociation of AOT or lecithin molecules. With increasing solute concentration a plateau conductivity is observed. This concentration range may be identified as cmc region. After micellization has occurred, a linear dependence of conductivity on solute concentration is observed and charged micelles are the predominant charge carriers. Only minute quantities of micelles are ionized. From a simple model the fraction of ionized micelles has been estimated to be 2.2×10^{-5} in the case of AOT and 2.13×10^{-3} in the case of lecithin. The mean value of $\alpha = 2.2 \times 10^{-5}$ obtained for the AOT hexadecane system is comparable to the data reported by Roberts et al. [2] for a NaAOT dodecane system ($\alpha = 1.5 \times 10^{-5}$). With a direct numerical simulation (DNS) of the PNP system the degree of dissociation has been extracted from the real lecithin system by a least squares fit. A degree of dissociation of about $\alpha = 0.5 \times 10^{-3}$ was obtained which is the same order of magnitude as compared to the simple model [1,6]. The results from the linear simulations are similar to the results of DNS but consume far less computational time. For high and moderate frequencies the model describes the impedance results very well. This is sufficient to extract meaningful data from the experiments. The experimental impedance data and the simulated impedance behavior show a semi-circular feature in the Cole–Cole representation, i.e. the system can be described by a simple *RC* circuit. For small frequencies, however, we observe that the impedance from a nonlinear simulation and the one from a linear simulation deviate from each other and the experiment. This is due to three reasons: First, very high ionic concentrations arise in the simulations near the capacitor plates. In the real system this would affect local viscosity. This effect is not considered by the PNP model. Second, the response of the system depends on the applied voltage in a nonlinear fashion and using higher harmonic modes in the experiment would increase the accuracy of the impedance response. The concept of linear response theory as well as the linear impedance have to be modified to describe the behavior of the electrolyte, e.g. steric effects have been considered by Kilic et al. [45]. Third, for low frequencies large forces act on the fluid. This can lead to instabilities. The assumption of a zero flow field is no longer justified. The change in charge carrier speciation was proven by temperature dependent conductivity measurements: a change in activation energy of conduction in the cmc region occurs. In the Al (dips)$_3$ hexadecane systems charge carriers are formed up to millimolal solute concentrations solely by dissociation and conductivity is proportional to the square root of the solute concentration. The predominant mechanism that increases conductivity with increasing temperature in the micellar systems is an increase in ion mobility due to decreasing solvent viscosity.

In the future we will characterize PNP systems in the presence of a fluid flow which implies a more complex capacitor geometry including the nonlinear relation between flow and charge transport.

Acknowledgments

This research was partly funded by the Bayerische Forschungsstiftung (BFS), Grant No. 813-08. Support by the Leibniz program of DFG is gratefully acknowledged by W. Peukert. The research of DP is funded by the DFG Research Center MATHEON Project C10. This is gratefully acknowledged.

Appendix A. Supplementary material

Supplementary data associated with this article can be found, in the online version, at http://dx.doi.org/10.1016/j.jcis.2012.07.051.

References

[1] M.F. Hsu, E.R. Dufresne, D.A. Weitz, Langmuir 21 (2005) 4881–4887.
[2] G.S. Roberts, R. Sanchez, R. Kemp, P.B.T. Wood, Langmuir 24 (2008) 6530–6541.
[3] S.K. Sainis, J.W. Merrill, E.R. Dufresne, Langmuir 24 (2008) 13334–13337.
[4] A.S. Dukhin, P.J. Goetz, J. Electroanal. Chem. 588 (2006) 44–50.
[5] C.E. Espinosa, Q. Guo, V. Singh, S.H. Behrens, Langmuir 26 (2010) 16941–16948.
[6] S. Reuter, S. Franke, J. Imaging Sci. Technol. 48 (2004) 319–323.
[7] I. Chen, J. Mort, Langmuir 13 (1997) 5036–5040.
[8] V.F. Lvovich, M.F. Smiechowski, Electrochim. Acta 51 (2006) 1487–1496.
[9] M.F. Smiechowski, V.F. Lvovich, J. Electroanal. Chem. 577 (2005) 67–78.
[10] B. Comiskey, J.D. Albert, H. Yoshizawa, J. Jacobson, Nature 394 (1998) 253–255.
[11] R.A. Holroyd, W.F. Schmidt, Annu. Rev. Phys. Chem. 40 (1989) 439–468.
[12] E. Knoesel, M. Bonn, J. Shan, T.F. Heinz, Phys. Rev. Lett. 86 (2001) 340–343.
[13] J. Kim, J.L. Anderson, S. Garoff, L.J.M. Schlangen, Langmuir 21 (2005) 8620–8629.
[14] K. Neyts, F. Beunis, F. Strubbe, M. Marescaux, B. Verboven, M. Karvar, A. Verschueren, J. Phys.: Condens. Matter 22 (2010) 494108.
[15] H.F. Eicke, H. Christen, Helv. Chim. Acta 61 (1978) 2258–2263.
[16] M.B. Mathews, E. Hirschhorn, J. Colloid Sci. 8 (1953) 86–96.
[17] T.K. De, A. Maitra, Adv. Colloid Interface Sci. 59 (1995) 95–193.
[18] H. Cohen, J. Cooley, Biophys. J. 5 (1965) 145–162.
[19] T.R. Brumleve, R.P. Buck, J. Electroanal. Chem. 90 (1978) 1–31.
[20] W. Kucza, M. Danielewski, A. Lewenstam, Electrochem. Commun. 8 (2006) 416–420.
[21] J. Lim, J. Whitcomb, J. Boyd, J. Varghese, J. Colloid Interface Sci. 305 (2007) 159–174.
[22] A. Öchsner, G.E. Murch, Diffus. Defect Data, Pt. B 273 (2008) 113–118.
[23] H. Eicke, V. Arnold, F. L'Eplattenier, Angew. Chem., Int. Ed. 11 (1972) 1097–1098.
[24] F. Greenaway, L. Norris, Inorg. Chim. Acta 145 (1988) 279–284.
[25] L. Tavadyan, H. Tonikyan, S. Minasyan, L. Harutyunyan, F. Greenaway, S. Willimas, R. Gray-Kaufmann, J. Sorenson, Inorg. Chim. Acta 328 (2002) 1–12.
[26] G.L. Jendrasiak, Chem. Phys. Lipids 4 (1970) 85–95.
[27] J.W. Nichols, J. Ozarowski, Biochemistry 29 (1990) 4600–4606.
[28] Blei, R.E. Lee, J. Phys. Chem. 67 (1963) 2085–2088.
[29] P.H. Elworthy, D.S. McIntosh, J. Phys. Chem. 68 (1964) 3448–3452.
[30] F. Aliotta, M.E. Fontanella, M. Sacchi, C. Vasi, G.L. Manna, V. Turco-Liveri, Colloid Polym. Sci. 274 (1996) 809–818.
[31] S. Mackeben, M. Müller, C.C. Müller-Goymann, Colloids Surf., A 183–185 (2001) 699–713.
[32] P. Schurtenberger, C. Cavaco, Langmuir 10 (1994) 100–108.
[33] M. Kotlarchyk, J.S. Huang, S.-H. Chen, J. Phys. Chem. 89 (1985) 4382–4386.
[34] M. Zulauf, H.-F. Eicke, J. Phys. Chem. 83 (1979) 480–486.
[35] H. Saad, Y.C. Bae, E. Gulari, Langmuir 4 (1988) 63–66.
[36] S.S. Narayanan, S.S. Sinha, R. Sarkar, S.K. Pal, J. Phys. Chem. B 112 (2008) 2859–2867.
[37] F. Keller, M. Feist, H. Nirschl, W. Dörfler, J. Colloid Interface Sci. 344 (2010) 228–236.
[38] D. Franceschetti, J. Macdonald, J. Electroanal. Chem. 101 (1979) 307–316.
[39] C. Lubich, A. Ostermann, IMA J. Numer. Anal. 15 (1995) 555–583.
[40] C. Lubich, A. Ostermann, Math. Comput. 64 (1995) 601–627.
[41] A. Ostermann, M. Roche, Math. Comput. 59 (1992) 403–420.
[42] A. Ostermann, M. Roche, SIAM J. Numer. Anal. 30 (1993) 1084–1098.
[43] C. Curtiss, J. Hirschfelder, Proc. Natl. Acad. Sci. U.S.A. 38 (1952) 235–243.
[44] R. Alexander, SIAM J. Numer. Anal. 14 (1977) 1006–1021.
[45] M.S. Kilic, M.Z. Bazant, A. Ajdari, Phys. Rev. E 75 (2007) 021503.